


# The Morcles microgranite (Aiguilles Rouges, Swiss Alps): geochronological and geochemical evidences for a common origin with the Vallorcine intrusion

Denise Bussien Grosjean<sup>1</sup>  · Nicolas Meisser<sup>1</sup> · Sylvie May-Leresche<sup>2</sup> · Alexey Ulianov<sup>3</sup> · Pierre Vonlanthen<sup>3</sup>

Received: 2 December 2016 / Accepted: 3 September 2017 / Published online: 20 September 2017  
© Swiss Geological Society 2017

**Abstract** The Morcles microgranite is located in the N–E termination of the Aiguilles Rouges massif (External Crystalline Massifs, Switzerland). It outcrops as dykes, a few meters to 150 m in thickness, intruding the Aiguilles Rouges polymetamorphic basement, and presents variation of texture from granophyric to rhyolitic. We present here for the first time, in situ U–Pb zircon dating of the Morcles microgranite/rhyolite based on laser-ablation—inductively coupled plasma—mass spectrometry (LA-ICP-MS) data. Results indicate late Variscan emplacement ages at ~303 and ~309–312 Ma, a major Caledonian inherited component age at ~445–460 Ma, and secondary inherited ages ranging from Pan-African (550–1000 Ma) to Paleoproterozoic (2.3 Ga). Geochronological and geochemical data indicate that the Morcles microgranite/rhyolite shares a common origin with the higher (or “H”) facies of the neighbouring Vallorcine granitic intrusion. This close affinity is further corroborated by the geographical alignment of both intrusive bodies on either side of the Rhone Valley. The fine-grained texture of the microgranite groundmass and the rhyolite indicates a very rapid cooling

rate and emplacement close to the surface, suggesting that the Morcles microgranite/rhyolite may constitute the shallow-level counterpart of the Vallorcine granite. The mineralogical assemblages observed in the Morcles microgranite/rhyolite support the idea of high-temperature melting conditions provided by underplating of mantle-derived magmas during the Carboniferous extension of the Variscan cordillera.

**Keywords** Zircon U–Pb dating · Aiguilles Rouges massif · Vallorcine intrusion · Late-Variscan magmatism

## 1 Introduction

The Aiguilles Rouges (AR) massif is one of the External Crystalline Massifs (ECMs) of the Alps belonging to the European continental crust. The ECMs mainly consist in a pre-Mesozoic basement intruded during the Variscan collisional orogenic event by numerous magmatic plutons, mostly Carboniferous in age (e.g. Schaltegger and Gebauer 1999; Schaltegger et al. 2003; von Raumer et al. 2013). The genesis and emplacement of those intrusions occurred during the Variscan collision involving Laurussia, the Gondwana-derived Avalonia and Hunia superterrane, and Gondwana itself, which followed the successive closure of the Rheic, the Rhenohercynian and the Paleotethys oceans, at least (Stampfli et al. 2013). The Lower Carboniferous plutons (~330 Ma) are associated with the northwards subduction of the Paleotethys ridge beneath the block formed by the Hunia superterrane and Laurussia (Stampfli et al. 2011), whereas the Upper Carboniferous plutons (~300 Ma) emplaced in an rifting context either by transpression (e.g. Corsini and Rolland 2009; Rolland et al. 2009), or slab roll-back (e.g. Faure et al. 1997; Stampfli

Editorial handling: E. Gnos.

**Electronic supplementary material** The online version of this article (doi:10.1007/s00015-017-0282-3) contains supplementary material, which is available to authorized users.

✉ Denise Bussien Grosjean  
denise.bussien.grosjean@gmail.com

- <sup>1</sup> Musée Cantonal de Géologie, UNIL-Anthropole, 1015 Lausanne, Switzerland
- <sup>2</sup> Chemin de Sur Ville, 1136 Bussy-Chardonney, Switzerland
- <sup>3</sup> Institut des Sciences de la Terre, UNIL-Géopolis, 1015 Lausanne, Switzerland

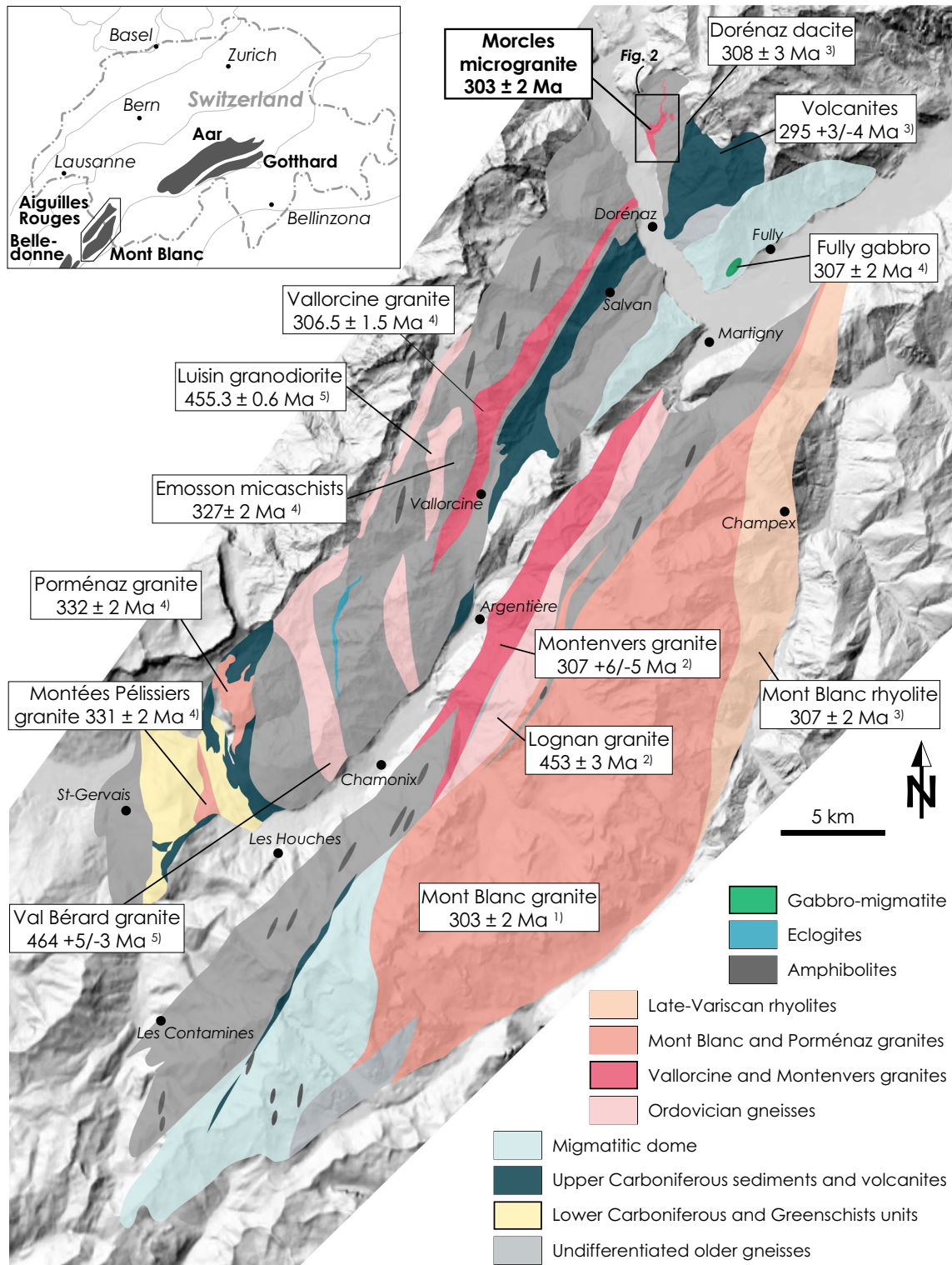


**Fig. 1** Simplified geological map of the Aiguilles Rouges and Mont Blanc massifs modified from Morard and von Raumer (2005), with the position of the Morcles microgranite. U–Pb ages for the different intrusions are from: (1) Bussy and von Raumer (1993), (2) Bussy and von Raumer (1994), (3) Capuzzo and Bussy (2000), (4) Bussy et al. (2000), (5) Bussy et al. (2011). The digital elevation model (DEM) is

from the Atlas de la Suisse (Version 1.0.62.2 ©2017, Institute of Cartography and Geoinformation, ETH Zurich, [www.atladerschweiz.ch](http://www.atladerschweiz.ch)). The inset shows the position of both massifs in the Swiss Alpine arc, along with other External Crystalline Massifs (in dark grey), and relative to the Jura, Plateau, Helvetic and Penninic domains (from North to South, light grey lines)

et al. 2013). Most of the Carboniferous plutons (Fig. 1) are well preserved, and were only slightly affected by the greenschist facies Alpine metamorphism (von Raumer and Bussy 2004).

At the end of the 1980s the construction of roads in the Morcles area (northernmost part of the AR massif) gave access to new outcrops of microgranitic dykes. Chemical analyses were carried out already in the early 1990s but the question remains as to whether this microgranite is genetically distinct, or related to other intrusive bodies of the AR massif. The goal of this study is to uncover the origin of the Morcles microgranite based on in situ U–Pb zircon dating and major, minor, and trace element geochemical data. Comparison of our data with those already available for several intrusive bodies in the neighbourhood allows us to demonstrate the genetic relationship between the Morcles microgranite and the Vallorcine granitic intrusion.

## 2 Geological framework

The AR massif is one of the westernmost ECMs outcropping in the Swiss Alps (Fig. 1). Along with the neighbouring Mont Blanc (MB) massif, with which it shares a similar geological history, the AR massif represents a window on the pre-Mesozoic basement of the European crust. Both underwent several orogenic cycles recorded throughout Alpine basements, including a late-Cambrian–Ordovician orogenic cycle (e.g. Schaltegger 1993; Schaltegger and Gebauer 1999; Guillot et al. 2002; Scheiber et al. 2014) and the Variscan high-grade metamorphic event, which led to extensive migmatitisation (von Raumer 1998; von Raumer et al. 1999). Often referred to as undifferentiated and polymetamorphic, the basement of the AR–MB massifs comprises a wide spectrum of lithologies including orthogneiss, amphibolite, eclogite, metagreywacke, micaschist, paragneiss, quartzite and marble, all typical of the Variscan metamorphic basement observed in Central Europe (von Raumer 1998, von Raumer et al. 2013). The pre-Mesozoic basement of the AR massif also contains in its southern part the so-called Greenstone Unit, which is formed of calc-alkaline volcanic rocks, and Viséan sediments (metagreywackes, schists) interbedded with metabasalts (Dobmeier 1996; Dobmeier et al. 1999).

The influence of the Alpine orogeny on the rocks forming the AR–MB massifs was rather limited. Even though there is no doubt that the large-scale antiform structure formed by the present-day AR–MB massifs was shaped by the Alpine cycle (e.g. von Raumer and Bussy 2004; Rolland et al. 2008; Egli and Mancktelow 2013; Boutoux et al. 2016; Egli et al. 2017), rock deformation remained weak or localised within shear zones. The mineral assemblages were only slightly affected by Alpine

metamorphism which hardly reached the greenschist facies (von Raumer 1969; von Raumer et al. 2009, and reference therein). The geological framework of the AR–MB massifs can therefore be summarised as an assemblage of Precambrian to lower Palaeozoic sedimentary and magmatic rocks, strongly metamorphosed during the Variscan high-grade metamorphic event, and later intruded by late-Variscan plutons, which were only weakly metamorphosed and deformed during the Alpine cycle.

On a larger scale, the intrusions of the AR massif are stretched towards two main geographical directions (Fig. 1). The first one, oriented N–S, is underlined by the Viséan Montées Pélissier and Porménaz granites. The second one, oriented NE–SW, is highlighted by the Ordovician Luisin granodiorite, the Carboniferous Vallorcine granite and Salanfè rhyolitic dykes. The NE–SW trend is further reinforced by the Salvan–Doréaz synform, an elongated basin filled with a Carboniferous dacite and Permian volcanoclastic/siliciclastic sediments, and later pinched between basement units during the Alpine orogeny. The NE–SW orientation also prevails for the granitic intrusions of the MB massif, namely the Ordovician Lognan and the Carboniferous Montenvers/Mont Blanc plutons.

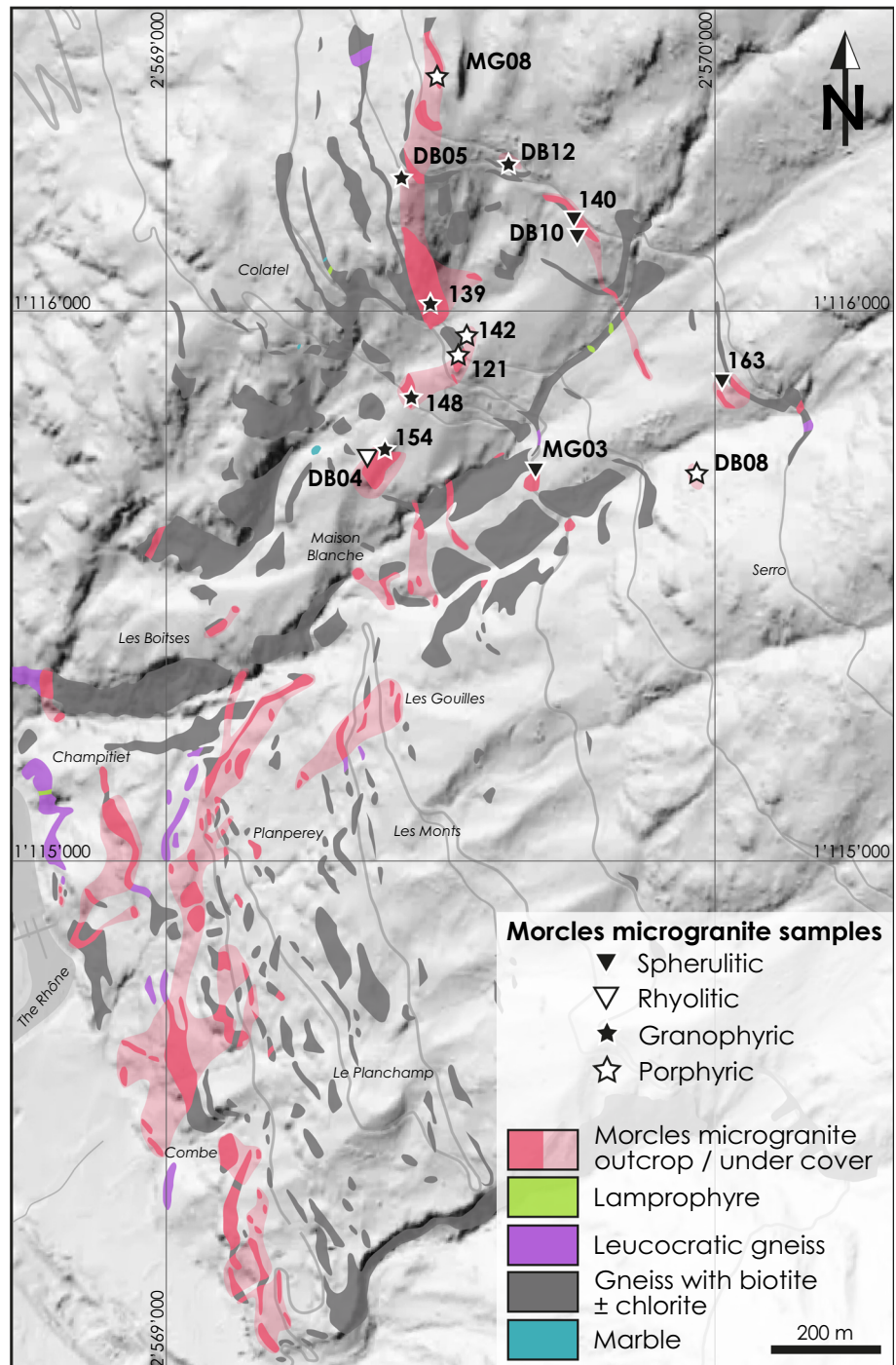
Small-volume intrusions have been reported in the north-eastern part of the AR massif, on both sides of the Salvan–Doréaz synform. In the north, the Morcles microgranite, a dacitic flow, and lamprophyres (Fig. 2) have been described in previous pieces of work (Leresche 1992; Capuzzo and Bussy 2000; Mollex 2003), while in the south, the Fully gabbro-migmatites, composed of peraluminous migmatitic granitoids and gabbroic enclaves (Mollex 2003), have been dated at  $307 \pm 2$  Ma (Bussy et al. 2000). Geochronological and geochemical data point to a genetic link between the Fully granitoids and the basal dacite of the Salvan–Doréaz basin (Mollex 2003). Comparisons between the Fully gabbro-migmatite and the Morcles lamprophyres have also been made, but no direct genetic link could be documented (Mollex 2003). It is not known either, whether the Morcles microgranite is genetically distinct or related to other intrusive bodies of the AR massif. The new geochronological and geochemical data presented here are aimed at addressing this issue.

## 3 Samples

The Morcles intrusive bodies outcrop as grey, sometimes bluish, microgranitic dykes (together with rare dacite and lamprophyre), oriented almost vertically in the N–S direction (Fig. 2). The outcrop exposure is generally poor, the full extent of the dykes becoming obvious at the scale of the map only (Fig. 2). The thickness of the dykes, which



**Fig. 2** Detailed geological map of the Morcles area with the microgranite outcrops (solid colour) and under Quaternary cover (transparent colour). For a description of sample textures, see Table 1. DEM as in Fig. 1



can easily be underestimated due to the presence of the Quaternary cover, varies from a few metres in the higher N–E area to 150 m in the lower S–W region. They crosscut the leucocratic gneiss and the biotite gneiss of the poly-metamorphic basement. The contact with both gneisses is generally sharp, but it may sometimes also contain a centimetre thick band of darker minerals. Although they underwent Alpine metamorphism, the dykes are only slightly deformed, if at all. The mineral assemblage

contains several types of phenocrysts (0.5–10 mm), including partially corroded quartz, extensively sceriticised orthoclase, perthitic plagioclase (~5% An), and slightly ferro-magnesian muscovite. The plagioclase was firstly altered in biotite, which was later transformed in ferri-ferrous chlorite or seldom chamosite. The phenocrysts are embedded in a fine-grained groundmass (0.1–0.5 mm) composed of quartz, white mica (magmatic and metamorphic), and cordierite partially or fully pseudomorphosed (or

**Table 1** List of Morcles microgranite samples analysed with corresponding outcrop location (Swiss grid coordinates), rock texture and analyses carried out

Samples	Swiss grid coordinates		Texture	Type of analyses
	X (m)	Y (m)		
121	1'115'895	2'569'525	Porphyric	XRF, LA-ICP-MS trace elements
139	1'116'010	2'569'480	Granophyric	XRF, LA-ICP-MS trace elements
140	1'116'175	2'569'730	Spherulitic	XRF, LA-ICP-MS trace elements
142	1'115'920	2'569'550	Porphyric	XRF, LA-ICP-MS trace elements
148	1'115'810	2'569'450	Granophyric	XRF, LA-ICP-MS trace elements
154	1'115'740	2'569'400	Granophyric	XRF, LA-ICP-MS trace elements
163	1'115'850	2'570'065	Spherulitic	XRF, LA-ICP-MS trace elements
MG03	1'115'715	2'569'660	Spherulitic	XRF, LA-ICP-MS trace elements
MG08	1'116'400	2'569'500	Porphyric	XRF, LA-ICP-MS trace elements
DB04	1'115'730	2'569'370	Rhyolitic	LA-ICP-MS U/Pb dating
DB05	1'116'230	2'569'430	Granophyric	LA-ICP-MS U/Pb dating
DB08	1'115'660	2'569'970	Porphyric	XRF, LA-ICP-MS trace elements and U/Pb dating
DB10	1'116'145	2'569'745	Spherulitic	XRF, LA-ICP-MS trace elements and U/Pb dating
DB12	1'116'255	2'569'640	Granophyric	XRF, LA-ICP-MS trace elements and U/Pb dating

“pinitised”) into white mica and chlorite. Accessory minerals include zircon, fluorapatite, hematite, ilmenite, rutile, anatase, epidote, titanite, pyrite, galena, tennantite and native gold. Locally, the microgranite is crosscut and silicified by veins of Permo-Triassic age enriched in U, V, REE, and by late-stage Alpine veinlets rich in quartz, albite, anatase, and calcite (Meisser 2012). On the basis of textural criteria the microgranite can be classified as porphyric, spherulitic or granophyric (Table 1; Fig. 2). The porphyric texture (samples 121, 142, MG08, and DB08) is characterised by phenocrysts (quartz, K-feldspar, plagioclase) of various size embedded in a fine-grained foliated groundmass (0.1–0.5 mm). The spherulitic texture (samples 140, 163, MG03, and DB10) contains spherulites (up to 1 mm in size) of fibrous quartz and feldspar forming up to 90% of the groundmass. They surround quartz and feldspar phenocrysts, but also the smaller grains (0.5 mm) present in the groundmass. The granophyric texture (samples 139, 148, 154, DB05, and DB12) is identified through its coarser groundmass (0.5–1 mm), and the occurrence of symplectites and sparse sheaves of white mica. The texture of one sample (DB04) can even be qualified as rhyolitic with mm-sized rounded bipyramidal crystals of HT  $\beta$ -quartz (pseudomorphosed into  $\alpha$ -quartz during cooling) trapped in an aphanitic groundmass.

#### 4 Methods

Analytical work and microscope observation were performed at the Institute of Earth Sciences of the University of Lausanne (Switzerland). Whole rock chemical analyses of the Morcles microgranite were carried out on fused pellets using Philips PW 2400 and PANalytical

AXIOS <sup>mAX</sup> X-ray fluorescence spectrometers to quantify the major element composition of the samples. A GeoLas 200 M ArF excimer laser ablation system interfaces to an inductively coupled plasma–mass spectrometer (LA-ICP-MS) Agilent 7700 $\times$  was used on the same pellets to determine the trace element compositions. Operating parameters included a 120  $\mu$ m laser beam diameter, an on-sample energy density of  $\sim 5$  J/cm<sup>2</sup> and a repetition rate of 10 Hz. For the calibration of relative sensitivity factors, the NIST SRM 612 glass standard was used.

Classical mineral separation techniques were applied to extract zircon grains from five samples of microgranite (DB04, DB05, DB08, DB10 and DB12). After being crushed into powder, the rock samples were sieved and the zircon grains concentrated either in heavy liquids (bromofrom  $\rho = 2.89$  and methylene iodide  $\rho = 3.31$ ) or by panning. Zircon grains of gem quality were handpicked, mounted in epoxy resin, and polished to approximately half of their thickness. The methodology of Pupin (1980) was used throughout this study to classify zircon grains based on their morphology, but too few grains were extracted to obtain valid statistics to present them.

Before proceeding to zircon dating using LA-ICP-MS, panchromatic cathodoluminescence (CL) images were taken in order to adequately define the location of the laser spots. The grains were imaged using a CamScan MV 2300 SEM operated at an acceleration voltage of 10 kV, a probe current of 0.5 nA, and a working distance of  $\sim 40$  mm. Dating was performed using an Element XR (Thermo Scientific) ICP-MS coupled with a NewWave UP-193FX 193 nm ArF excimer laser system (ESI) using a pulse repetition rate of 5 Hz, an on-sample energy density of  $\sim 3$  J/cm<sup>2</sup>, and analytical conditions very similar to those described by Ulianov et al. (2012). The analytical spot

diameter varied between of 25 and 35  $\mu\text{m}$  according to grain size and growth structure complexity. Accuracy and relative sensitivity were assessed against Plešovice (Sláma et al. 2008) and GJ-1 (Griffin et al. 2004; Jackson et al. 2004) natural zircon standards, respectively. Raw data were processed offline using the LAMTRACE software (Jackson 2008). The Concordia diagrams showing the ages calculated from U–Pb isotope ratios and U–Pb frequency plots were generated using the Isoplot/Ex v. 4.15 software (Ludwig 2012). The concordant age obtained for the Plešovice zircon standard ( $337.09 \pm 0.85$  Ma,  $2 \sigma$  error,  $n = 20$ ) is identical (within analytical uncertainty) to the reference age ( $337.13 \pm 0.37$  Ma, Sláma et al. 2008).

## 5 Results

### 5.1 Geochemistry of the Morcles microgranite

Despite the textural differences, the Morcles microgranite samples have very similar chemical compositions (Table 2; Figs. 3, 4), and have been barely altered by Alpine metamorphism. The high contents of  $\text{SiO}_2$  (71.00–73.32 wt%),  $\text{K}_2\text{O}$  (4.26–5.27 wt%),  $\text{Al}_2\text{O}_3$  (14.04–14.91 wt%), and Ba (228–690 ppm) point to an evolved chemical composition and correlate well with the high modal abundance of K-feldspar and white mica. The Mg# (Mg number in molar) is low (30–38), as are the contents of  $\text{TiO}_2$  (0.13–0.41 wt%), MgO (0.24–0.73 wt%), CaO (0.54–1.15 wt%), and  $\text{Na}_2\text{O}$  (3.02–4.11 wt%). The predominance of K-feldspar over plagioclase is in line with the high contents of  $\text{K}_2\text{O}$ , Rb, and Ba, and the rather low values of  $\text{Na}_2\text{O}$ , CaO and Sr. With respect to their alkali content, the three textural types of the Morcles microgranite can all be classified as high-K alkaline to slightly calc-alkaline. The aluminium saturation index ( $A/\text{CNK} > 1.1$ ), coupled with relatively high values of  $\text{P}_2\text{O}_5$  (0.33–0.38 wt%), points to peraluminous affinities (S-type granite). MgO is positively correlated with FeO,  $\text{TiO}_2$ , Sr, Zr and the transition elements V, Cr and Ni, whereas V is negatively correlated with  $\text{SiO}_2$  (Fig. 3). Concentrations of incompatible elements such as U, Th, Hf, Nb, Y and Zr are also rather low.

Rare earth element (REE) patterns also share many similarities between the three sample types (Fig. 4). Despite the moderate abundance of plagioclase all samples present a medium to strong negative Eu anomaly (0.66–0.36). Fractionation is stronger for the light REE (LREE) than the heavy REE (HREE) [ $(\text{La}/\text{Sm})_N - (\text{Gd}/\text{Lu})_N = 0.2$  to 1.6], except for the two spherulitic samples 140 and 163 (–0.1). Sample 163 presents the highest enrichment in LREE and middle REE, whereas porphyric sample 121 contains the lowest REE concentrations.

### 5.2 U–Pb zircon dating

Zircon dating has provided both concordant and discordant ages. The strongly discordant measurements were ascribed to analytical errors (e.g. overlap with misidentified inherited cores). Such measurements were discarded and not considered for interpretation. Only concordant ages and discordant ages fitting with the Discordia line were taken into account (Fig. 5; Supplementary Table 3). Despite those precautions, calculated concordant ages (within  $2 \sigma$  error) were difficult to obtain (see the high MSWD values in Fig. 5), because only small clusters of grains ( $n$  varies between 4 and 9) presenting similar resulting age were selected for the calculation. The analyses emphasise the presence of inherited zircon cores incorporated from the wall rock during the emplacement of the dykes. Rapid magma cooling and crystallisation are the main reasons why many zircon cores escaped full resorption.

The zircon grains separated from the five samples selected for dating are very similar. They are pinkish, of gem quality, and inclusion-poor. Most of them show an elongated shape (2:1 aspect ratio) with morphologies typical of peraluminous granite (S7, S11, S12). The CL images of most zircon grains reveal complex internal growth microstructures, with well-developed magmatic oscillatory zoning surrounding a partially resorbed inherited core. Sector zoning is frequently observed along with oscillatory zoning, as are thin non-luminescent rims interpreted as metamorphic overgrowths (Fig. 6).

The rhyolitic sample DB04 (Fig. 6, grain [18]) did not provide a coherent Concordia age of crystallisation. The  $^{206}\text{Pb}/^{238}\text{U}$  apparent age distribution diagram shows several major peaks at 304, 309 and 453 Ma, and minor ones at 271, 400 and 640 Ma (Fig. 5g). The peak at 304 Ma is interpreted as the crystallisation age, whereas the slightly discordant age at 271 Ma is obtained from slightly fractured zircon grains possibly subject to Pb loss. The older ages are attributed to zircon inheritance.

Sample DB05 contains grains with partially resorbed inherited cores (Fig. 6, grain [77]). Ages obtained from the magmatic overgrowths form clusters either at  $310.9 \pm 2.1$  Ma (MSWD = 3.0, 4 analyses), or at  $453.6 \pm 1.8$  Ma (MSWD = 3.7, 9 analyses; Fig. 5a, d). Inherited cores present a wide range of ages with peaks at 515, 626, 740, and 970 Ma, and for two grains, at 1.0 and 2.3 Ga (Fig. 5h). A few grains give slightly discordant younger ages, despite any obvious disturbances of the CL microstructure. The age of  $310.9 \pm 2.1$  Ma could be attributed to the emplacement of the microgranite, but 3 zircons give a calculated Concordia age of  $302.4 \pm 1.3$  Ma (MSWD = 0.98, not shown, see Supplementary Table 3). The older ages, including the peak at 454 Ma (Fig. 5h), and hence the calculated age at  $453.6 \pm 1.8$  Ma, are inherited

**Table 2** Whole rock XRF and LA-ICP-MS analyses (Institute of Earth Sciences, University of Lausanne, Switzerland) for the Morcles microgranite samples listed in Table 1

Morcles microgranite												
Texture	Porphyric				Spherulitic				Granophyric			
Sample	DB08	MG08	121	142	DB10	MG03	140	163	DB12	139	148	154
SiO <sub>2</sub>	71.00	71.58	73.32	72.25	72.00	72.74	71.39	70.61	71.60	73.03	72.11	71.63
TiO <sub>2</sub>	0.29	0.31	0.13	0.22	0.26	0.24	0.29	0.41	0.29	0.26	0.25	0.31
Al <sub>2</sub> O <sub>3</sub>	14.63	14.80	14.66	14.66	14.89	14.35	14.81	14.91	14.56	14.04	14.76	14.84
Fe <sub>2</sub> O <sub>3</sub>	1.60	0.61	0.45	0.38	0.32	0.33	0.60	0.60	0.24	0.36	0.64	0.31
FeO	0.33	1.26	0.42	1.08	1.29	1.13	1.18	1.55	1.48	1.09	0.98	1.48
MnO	0.03	0.03	0.03	0.05	0.03	0.03	0.04	0.04	0.03	0.03	0.03	0.03
MgO	0.50	0.57	0.24	0.34	0.45	0.36	0.54	0.73	0.47	0.42	0.41	0.43
CaO	1.15	0.74	0.59	0.75	0.54	0.60	0.66	0.67	0.60	0.58	0.58	0.58
Na <sub>2</sub> O	3.29	3.52	4.11	3.82	3.55	3.79	3.31	3.39	3.45	3.29	3.38	3.02
K <sub>2</sub> O	5.10	4.93	4.26	4.86	5.03	5.07	5.11	5.19	5.16	4.77	5.21	5.27
P <sub>2</sub> O <sub>5</sub>	0.33	0.38	0.37	0.33	0.34	0.34	0.36	0.38	0.34	0.33	0.34	0.35
H <sub>2</sub> O	0.82	1.04	0.81	0.88	1.05	0.71	1.25	1.19	1.31	0.96	0.95	1.02
CO <sub>2</sub>	0.59	0.14	0.16	0.27	0.16	0.18	0.11	0.14	0.18	0.17	0.14	0.16
Total	99.66	99.90	99.54	99.90	99.91	99.87	99.67	99.79	99.71	99.34	99.89	99.59
Mg#	33	36	34	30	33	31	36	38	33	34	32	30
A/CNK	1.12	1.19	1.18	1.13	1.21	1.12	1.21	1.20	1.18	1.21	1.20	1.27
Sc	10.5	10.2	10.5	10.4	11.0	10.1	11.2	11.1	10.2	11.1	n.a.	n.a.
V	18.0	17.0	3.00	11.0	16.0	13.0	20.0	28.0	16.0	16.0	15.0	18.0
Cr	6.00	12.0	–	–	5.00	4.00	5.00	8.00	5.00	3.00	5.00	6.00
Co	49.7	49.8	41.8	42.1	48.0	44.5	40.9	38.5	72.3	69.1	47.0	40.0
Ni	4.19	4.45	<4	<4	4.45	5.35	3.25	4.06	3.24	5.06	–	–
Cu	22.2	7.89	30.4	34.5	15.6	15.5	8.90	10.6	10.3	16.5	–	–
Zn	92.3	96.1	69.1	84.0	82.4	71.5	89.9	92.8	81.6	98.8	71.0	31.0
Ga	20.0	22.0	23.0	19.0	20.0	17.0	20.0	21.0	21.0	21.0	23.0	22.0
Rb	255	296	339	281	308	245	273	287	303	306	306	321
Sr	103	93.8	60.6	83.9	84.7	77.6	97.0	114	81.6	95.7	77.0	86.0
Y	15.7	14.2	11.4	11.9	14.1	17.9	14.8	15.8	13.5	11.8	13.0	15.0
Zr	121	119	57.2	85.5	105	99.8	114	157	122	107	113	131
Nb	18.4	18.0	21.4	17.5	18.0	18.0	16.7	17.1	17.1	18.2	5.00	–
Cs	9.45	12.6	27.0	11.3	10.8	9.49	11.2	11.8	10.3	16.2	n.a.	n.a.
Ba	614	347	273	336	517	416	577	485	365	690	228	251
La	22.6	22.3	10.4	15.3	13.8	20.4	20.9	32.1	23.1	20.5	18.0	23.0
Ce	47.7	47.5	19.6	32.6	32.2	42.2	43.5	68.5	50.3	45.2	47.0	47.0
Pr	5.43	5.47	2.50	3.74	3.50	4.87	5.12	7.94	5.94	5.17	n.a.	n.a.
Nd	20.4	21.0	9.22	14.6	13.1	19.4	19.1	30.3	22.4	20.0	17.0	20.0
Sm	4.23	4.31	2.24	3.01	3.19	4.15	4.36	6.08	4.63	3.90	n.a.	n.a.
Eu	0.57	0.56	0.37	0.35	0.46	0.77	0.63	0.67	0.48	0.42	n.a.	n.a.
Gd	3.43	3.66	1.84	2.40	2.72	3.03	3.59	4.77	3.56	3.12	n.a.	n.a.
Tb	0.53	0.53	0.27	0.35	0.40	0.47	0.51	0.62	0.47	0.43	n.a.	n.a.
Dy	2.89	2.70	1.70	2.05	2.37	3.02	2.52	3.10	2.51	2.22	n.a.	n.a.
Ho	0.49	0.48	0.28	0.32	0.41	0.55	0.43	0.48	0.40	0.38	n.a.	n.a.
Er	1.23	1.03	0.83	0.95	1.15	1.64	1.18	1.30	1.00	0.90	n.a.	n.a.
Tm	0.18	0.15	0.13	0.13	0.15	0.28	0.17	0.17	0.15	0.15	n.a.	n.a.
Yb	1.26	0.97	0.82	0.90	1.06	1.68	0.95	1.19	0.93	1.02	n.a.	n.a.
Lu	0.17	0.15	0.14	0.13	0.14	0.25	0.15	0.17	0.15	0.15	n.a.	n.a.

**Table 2** continued

Marcles microgranite												
Texture	Porphyritic				Spherulitic				Granophytic			
Sample	DB08	MG08	121	142	DB10	MG03	140	163	DB12	139	148	154
<i>Hf</i>	3.49	3.42	2.05	2.45	2.88	2.95	3.12	4.30	3.39	3.02	2.00	–
<i>Ta</i>	4.11	4.09	6.47	4.15	4.02	4.08	3.43	3.07	4.73	6.18	n.a.	n.a.
<i>Pb</i>	22.0	24.7	12.1	11.9	18.6	14.1	17.1	22.0	19.0	18.6	13.0	–
<i>Th</i>	11.8	10.9	5.92	8.48	10.8	10.2	10.0	18.0	13.8	12.1	5.00	6.00
<i>U</i>	8.76	8.96	10.9	12.1	9.09	9.69	8.27	8.46	8.43	6.86	6.00	–

Major elements (in wt%) and trace-elements (in ppm) measured by XRF and LA-ICP-MS (*in italics*), n.a. for not analysed Mg# and Aluminium saturation index (A/CNK) in molar

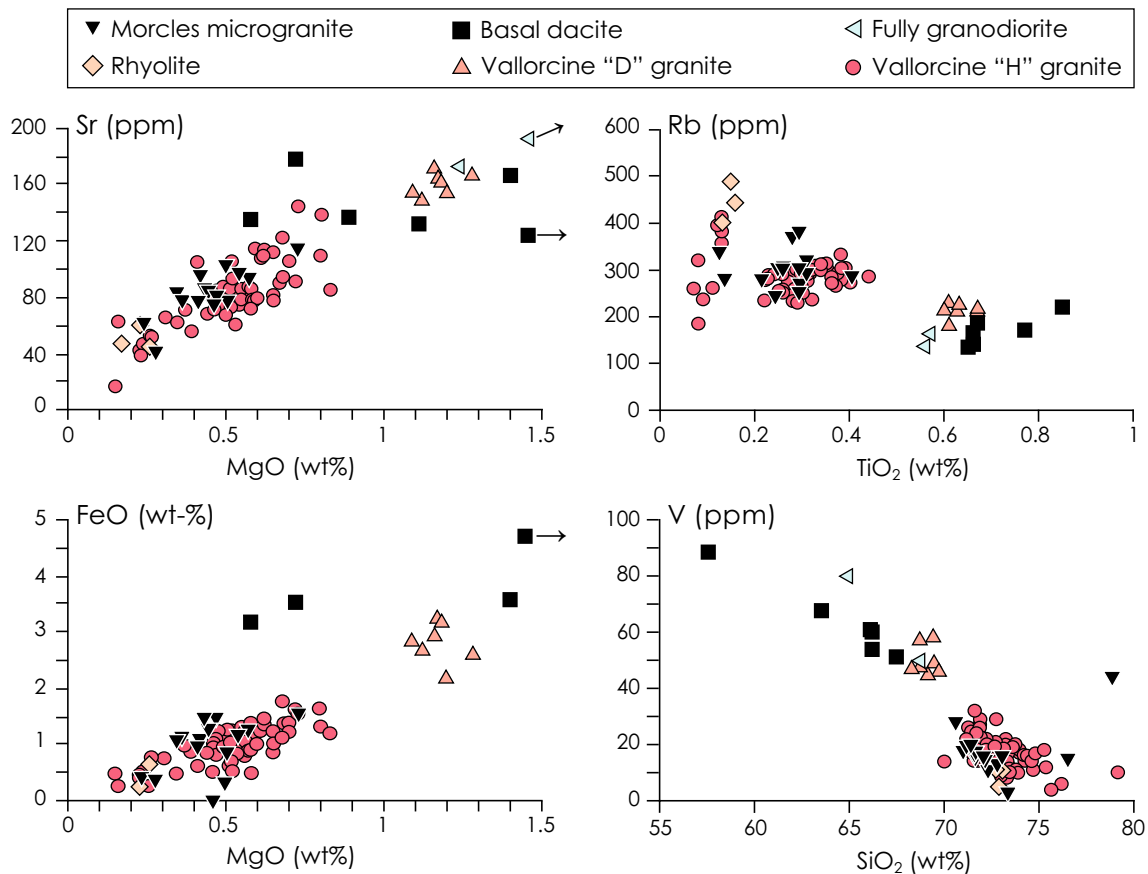


**Fig. 3** Harker diagrams of selected chemical elements for the Morcles microgranite (this study and Meisser 2003) compared to literature data for other contemporaneous intrusive bodies: the Dorénaz basal dacite (Pilloud 1991; Capuzzo and Bussy 2000;

Mollex 2003), the Aiguilles Rouges rhyolites (Capuzzo and Bussy 2000; Meisser 2003), the Fully granodiorite (Mollex 2003), and the Vallorcine “D” and “H” granites (Brändlein 1991; Brändlein et al. 1994; Meisser 2003)

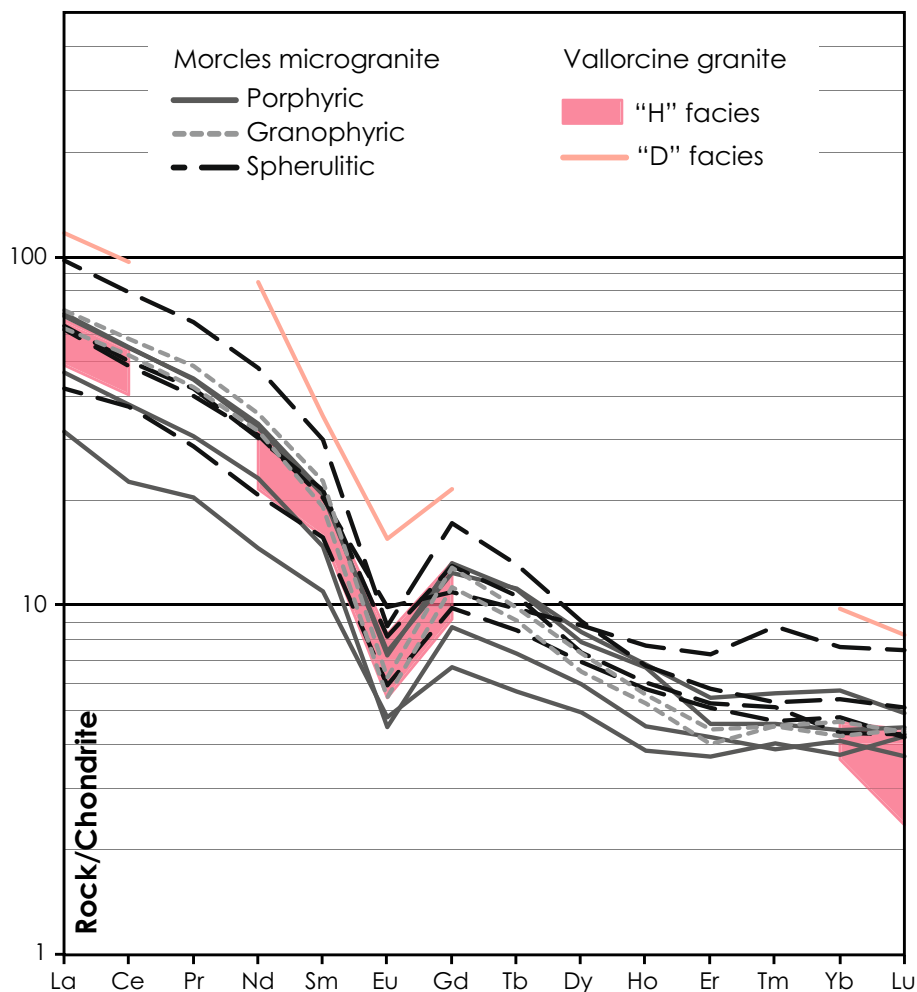
components. The younger values (<295 Ma) most likely result from Pb loss along fractures or other fast diffusion pathways.

Several grains from sample DB08 contain an inherited core, but only a few of them show complex internal microstructures (Fig. 6, grain [92]). The age distribution

diagram (Fig. 5i) shows a strong peak at 303 Ma, coherent with the Concordia age of  $302.5 \pm 3.0$  Ma (MSWD = 3.4,  $n = 6$ ; Fig. 5e), and a second one at 464 Ma. A third peak is observed at 520 Ma on the distribution diagram (Fig. 5i). An inherited core gives the oldest age of the sample at 815 Ma (Fig. 5i; Supplementary Table 3). The concordant



**Fig. 4** Chondrite-normalised REE diagram for the Morcles microgranite (this study) and the Vallorcine granite (Brändlein 1991; Brändlein et al. 1994). Chondritic reference values from Nakamura (1974) and Boynton (1984)



$302.5 \pm 3.0$  Ma age is interpreted as the crystallisation age, and older ages as inherited components.

Sample DB10 (Fig. 6, grain [101]) shows on the age distribution diagram a major peak at 309 Ma (no concordant age could be calculated), a smaller one at 459 Ma (corresponding to the cluster at  $457.7 \pm 3.7$  Ma in the Concordia diagram,  $\text{MSWD} = 0.106$ ,  $n = 5$ ; Fig. 5b), and minor peaks at 370, 630 and 705 Ma (Fig. 5j). The ages obtained for sample DB10 have not been affected by element remobilisation: the peak at 309 Ma corresponds to the magmatic emplacement of the microgranite, with a dominant inherited component at  $457.7 \pm 3.7$  Ma and some older cores.

Besides the classical morphologies typical of peraluminous granites (Pupin 1980), sample DB12 (Fig. 6, grain [138]) also contains the S19 morphological type of zircon, a feature suggesting possible calc-alkaline affinities (Pupin 1980). The ages range from 270 to 710 Ma, with peaks at 304, 312, 445, 575, and 630 Ma (Fig. 5k). The Concordia age at  $303.6 \pm 1.3$  ( $\text{MSWD} = 0.13$ , 4 analyses) corresponds to the magmatic emplacement, and the one at

$445.1 \pm 1.6$  Ma ( $\text{MSWD} = 0.31$ , 4 analyses) results from zircon inheritance. In this sample, the age at 270 Ma corresponds to analyses for which a thin outer rim was accidentally included in the analysis, which resulted in a decrease of the isotopic Pb/U ratios.

## 6 Discussion

### 6.1 U–Pb zircon ages of the Morcles microgranite

Despite the difficulties in calculating ages fitting with the Concordia ages, coherent ages pointing towards two major magmatic events, one in the Upper Carboniferous (late-Variscan) and one in the Ordovician (middle Caledonian), could be obtained from U–Pb zircon dating (see Fig. 5).

The Upper Carboniferous age is characterised by two peaks, one at  $\sim 303$  Ma (samples DB04, DB05, DB08, and DB12) and one at  $\sim 309$ – $312$  Ma (samples DB04, DB05, DB10 and DB12). In sample DB04, the peak corresponding to the younger age is slightly more prominent than the

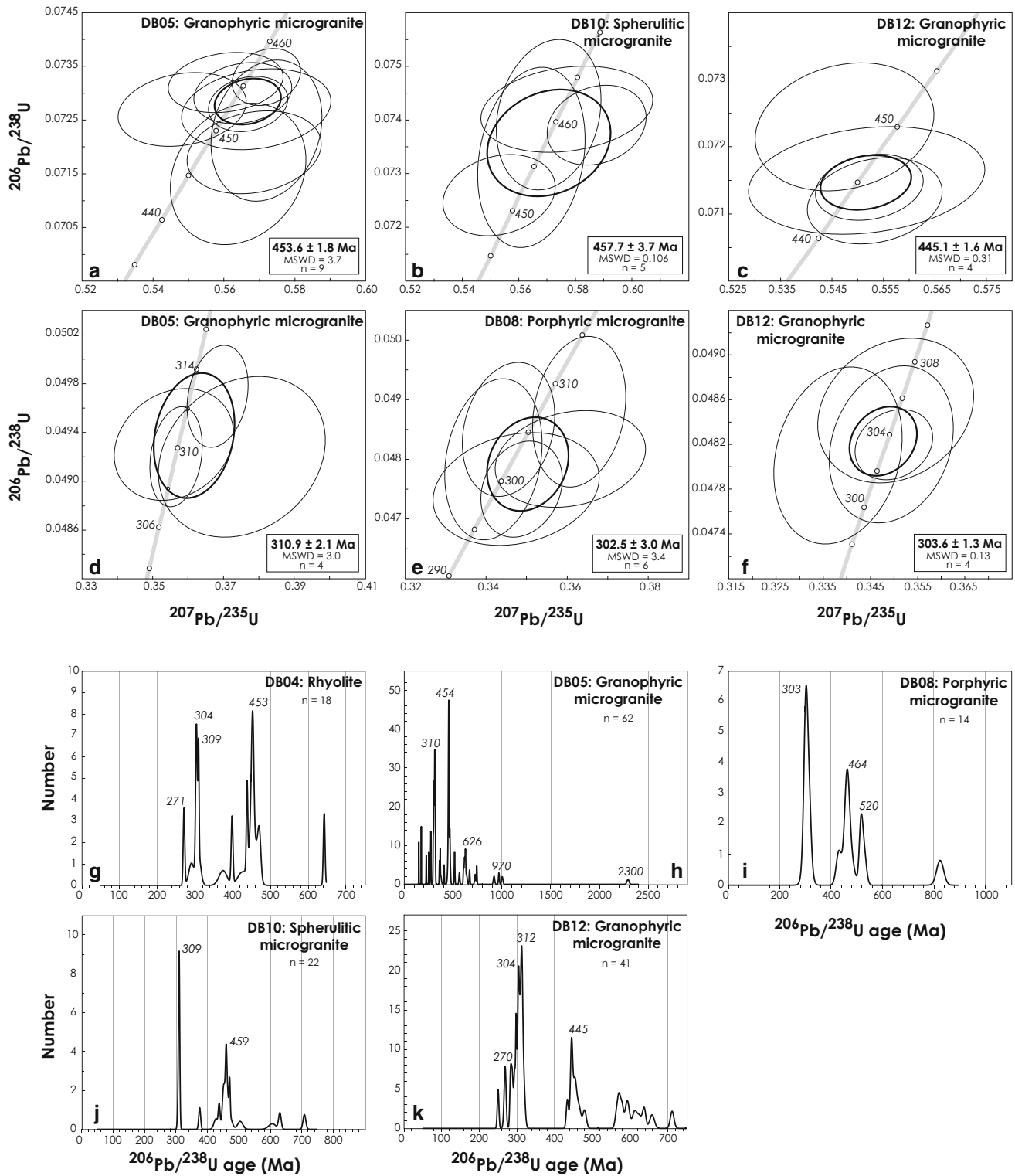


**Fig. 5** a–f Concordia diagrams of LA-ICP-MS U-Pb zircon analyses for the Morcles microgranite. Error ellipses represent  $2\sigma$  uncertainties. Ages of individual zircon grains are shown by thin ellipses, and the average age by a thick ellipse. The framed age is the Concordia

age obtained using the Isoplot software of Ludwig (2012); g–k  $^{206}\text{Pb}/^{238}\text{U}$  apparent age distributions (relative age-probability curves) for rhyolite and microgranite. The n value indicates the number of analyses used for each diagram

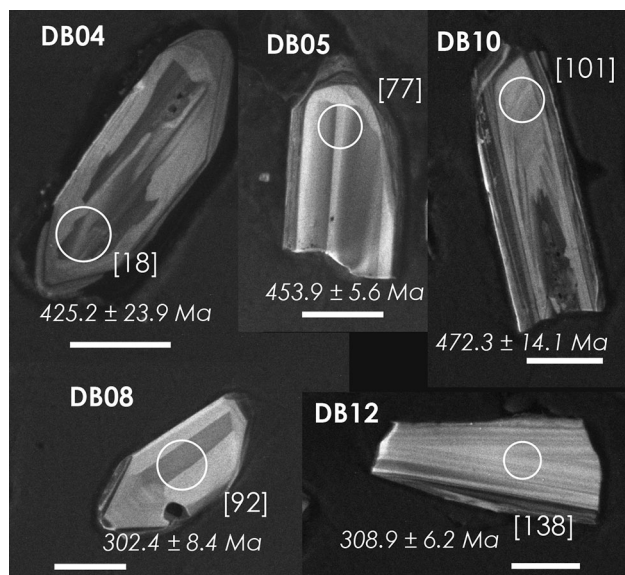


**Fig. 6** Panchromatic cathodoluminescence images of zircon grains separated from samples DB04 ([18]), DB05 ([77]), DB08 ([92]), DB10 ([101]) and DB12 ([138]) with location of LA-ICP-MS spots. Bracketed numbers correspond to analysis spots in Supplementary Table 3. The resultant  $^{206}\text{Pb}/^{238}\text{U}$  apparent ages are shown in italics with  $2\sigma$  errors. Scale bar represents 50  $\mu\text{m}$

older one, whereas in sample DB05, both calculated ages (Concordia ages of  $310.9 \pm 2.1$  and  $302.4 \pm 1.3$  Ma) are coherent but weak, the older being slightly more robust than the younger. Those contrasting results do not allow for an accurate and unequivocal determination of the emplacement age of the Morcles microgranite. Whatever the scenario, however, both peaks point to a late-Variscan emplacement of the microgranite, an interpretation coherent with the emplacement ages obtained for many other intrusive bodies found in the AR massif. Indeed, similar ages are reported for the Dorénaz basal dacite ( $308 \pm 3$  Ma, Capuzzo and Bussy 2000), the Fully gabbro-migmatite ( $307 \pm 2$  Ma, Bussy et al. 2000), the Vallorcine granite ( $306.5 \pm 1.5$  Ma, Bussy et al. 2000), and the Salvan-Dorénaz basin volcanites ( $295 +3/-4$  Ma, Capuzzo and Bussy 2000). The nearby MB massif is also largely constituted by late-Variscan intrusions (see Fig. 1), such as the Montenvers granite ( $307 +6/-5$  Ma, Bussy and von Raumer 1994), the Mont Blanc rhyolite ( $307 \pm 2$  Ma, Capuzzo and Bussy 2000), and the voluminous Mont Blanc granite ( $303 \pm 2$  Ma, Bussy and von Raumer 1993). The Western, Central and Southern Alpine basements also show widespread evidence for late-Variscan magmatism resulting from the collapse of the orogenic belt (see the review of Schaltegger and Gebauer 1999, Olsen et al. 2000).

The Ordovician age is characterised by peaks at  $\sim 453$  Ma (DB04 and DB05),  $\sim 458$  Ma (DB10), and  $\sim 464$  Ma (DB08). Similar ages were obtained for the

Luisin granodiorite ( $455.3 \pm 0.6$  Ma, Bussy et al. 2011), which lies approximately 15 km south of the Morcles intrusion (see Fig. 1), and further south, for the Val Bérard granite ( $464 +5/-3$  Ma, Bussy et al. 2011). In the case of the Morcles microgranite, the Ordovician age is interpreted as an inherited component coherent with the peraluminous affinity pointed by both geochemistry and zircon morphology. In this view, the AR basement itself, and especially its Ordovician intrusions, are part of the protolith. On a larger scale, Ordovician, magmatism, including the events occurring at  $\sim 455$  Ma, is well known through the Helvetic, Penninic, Austroalpine and Southern Alpine domains, for which a complete orogenic cycle is documented by a wide spectrum of rocks ranging from metagabbro to gneiss (Schaltegger and Gebauer 1999; von Raumer et al. 1999; Von Raumer et al. 2002; Schaltegger et al. 2003). Even though it is widely accepted that those magmatic events have been triggered by crustal extension of the northern Gondwanan margin, disagreements on the causes and magnitude of the extension still persist. Two geological settings are currently debated: (1) a back-arc context leading to the opening of either the Medio-European oceanic domain (Faure et al. 2009; Guillot and Ménot 2009) or the Galicia-Brittany ocean (Matte 2001, called the Galicia-Moldanubian ocean in Franke et al. 2017), or (2) a slab roll-back context giving rise to a partially aborted rift opening in the continuity of the Eastern Rheic ocean (Stampfli et al. 2013, von Raumer et al. 2013). The data of the present paper do not allow us to prioritize any of those two interpretations.

In addition to the peaks pointing to Upper Carboniferous and Ordovician ages, minor peaks are observed in partially resorbed zircon cores from several samples at  $\sim 630$ ,  $\sim 710$ ,  $\sim 970$ , and  $\sim 1000$  Ma (Fig. 5g–k). The age at  $\sim 630$ – $640$  Ma refers to the so-called “Pan-African zircons” regularly found in the Alpine basement (Gebauer 1993; Schaltegger 1993; Schaltegger and Gebauer 1999; Bussien et al. 2011) and correlated with the assembly of Gondwana (Veevers 2004; Rino et al. 2008; Bradley 2011). A very old zircon grain has been dated at 2.3 Ga, an age of Gondwanan affinity frequently reported in metasedimentary gneisses (Schaltegger and Gebauer 1999; Bertrand et al. 2000; Martínez Catalán et al. 2008, von Raumer et al. 2013).

The minor peaks at  $\sim 270$  Ma are coherent with an apparent age of  $256 \pm 18$  Ma obtained on an U-rich brecciated veinlet intruding the gneiss very close to the Salvan-Dorénaz synform (Pb/Pb dating, Meisser 2012). The 270 Ma perturbation could be ascribed to fluid circulation induced by the extension at the end of the Early Permian. This extension could be triggered by the fast exhumation of the rapidly eroded Variscan chain (Capuzzo and Wetzel 2004; Meisser 2012), leading even to local

magmatism observed in the Southern Alps (e.g. Schuster et al. 2001; Schaltegger and Brack 2007; Gretter et al. 2013).

## 6.2 Magma genesis and emplacement

Geochemistry and zircon morphology indicate that the origin of the Morcles microgranite results from the anatexis of the AR polymetamorphic basement, or, alternatively, from the melting of AR-derived sediments of the same age. Part of the heat required for partial melting may have been provided by intense shearing on major large-scale faults. However, the presence of cordierite in the microgranite points towards high-temperature melting conditions (Barbarin 1996), which cannot be explained solely by shearing. This point is further supported by the fact that the contemporaneous melting of large volumes of granodioritic magma, observed elsewhere in the Variscan belt, needs temperatures well above 800°. Such temperatures are obtained by large-scale dehydration of biotite, pointing towards dry melting conditions (Bussy et al. 2000). It is therefore thought that underplating of mantle-derived magmas provided most of the heat, an assumption supported by the occurrence of mafic enclaves in contemporaneous intrusions (e.g. Fully massif, Bussy et al. 2000, Mollex 2003; Mont Blanc massif, Bussy and von Raumer 1993). Underplating occurred in a context of extension of the Variscan lithosphere, the origin and setting of which are still debated. Common interpretations include (1) post-collisional re-equilibration (Rey et al. 1997), (2) lithospheric-scale, strike-slip displacement and faulting along a transpressive margin between Gondwana and Laurussia (Matte 2001; Corsini and Rolland 2009; Rolland et al. 2009), (3) thinning and spreading of the lithosphere above an asthenospheric plume (Franke et al. 2017), (4) formation of a back-arc basin (Faure et al. 1997), or (5) asthenospheric upwelling triggered by the roll-back and the detachment of the subducting slab, followed by the collapse of the Variscan edifice and the opening of the Paleotethys or Rhenohercynian oceans (Stampfli et al. 2013; Laurent et al. 2017). Whatever the scenario, this extensional regime favoured the intrusion of magmas as thin dykes. Only the last three settings, however, could account for a major involvement of a hot asthenospheric mantle.

The textures observed in the microgranite, ranging from granophyric, spherulitic, porphyric to rhyolitic, can be explained by the combined effects of cooling rate (itself dependent on the relative temperature of the magma and the host rock) and alteration. The porphyric and spherulitic textures likely result from the hydrothermal alteration of a rhyolitic glass, either immediately following crystallisation, during the Permian extension or during Alpine metamorphism (Cas and Wright 1987). In our samples,

both phenomena are documented by the magmatic alteration of feldspar and by the formation of alpine metamorphic minerals (chlorite, white mica) and veinlets (quartz, calcite, and chlorite). The occurrence of a rhyolitic texture points towards rapid cooling. However, as no lava flow has been observed among the Morcles intrusive bodies, a subsurface level of emplacement appears more realistic, even though no clear correlation can be made between the texture of the samples and their position within the dykes or the intrusion itself (see Fig. 2 for the location of the samples).

## 6.3 Affinity with other Aiguilles Rouges intrusions

The small volumes of microgranite outcropping in the Morcles area raise the question of a possible link with more voluminous contemporaneous intrusions in the AR basement. From a geochronological point of view, the Morcles microgranite could be related to the Fully gabbro-migmatite (Capuzzo and Bussy 2000; Mollex 2003), the Dorénaz basal dacite (Pilloud 1991; Capuzzo and Bussy 2000; Mollex 2003), and the Vallorcine porphyritic granite (Brändlein 1991; Brändlein et al. 1994; Bussy et al. 2000). An attempt to date an AR rhyolitic dyke from the Salanfe area has been made by Capuzzo and Bussy (2000), but zircon grains of average quality have only provided poorly constrained ages ranging between 294 and 307 Ma. In order to highlight the origin of the Morcles microgranite, the chemical data obtained in this study (Table 2) and in Meisser (2003) have been compared to the data collected from the above-mentioned intrusive rocks. From the Harker diagrams presented in Fig. 3, two groups can be distinguished: (1) the Fully granodiorite component of the gabbro-migmatite and the Dorénaz basal dacite (considered cogenetic by Mollex 2003), and the lower facies of the Vallorcine porphyritic granite (called “D” in Brändlein 1991) on one side, and (2) the AR rhyolites (geochemically analysed by Meisser 2012), the higher facies of the Vallorcine porphyritic granite (called “H” in Brändlein 1991) and the Morcles microgranite on the other side. In all four diagrams and in the  $\text{TiO}_2$  vs Rb one in particular, the systematic overlap of data suggests a strong chemical affinity between the Morcles microgranite and the Vallorcine “H” granite.

The common origin between the Morcles microgranite and the Vallorcine porphyritic “H” granite is further supported by their similar REE signatures (see Fig. 4). Although few REE data are available in the literature for the Vallorcine porphyritic “H” granite, they are clearly within the range (except for the element Lu) defined by the data we obtained for the Morcles microgranite. This is particularly obvious for the porphyric and granophyric textural types, and, to a lesser extent, for the spherulitic



type, which data overlaps the upper bound of the Vallorescine “H” data. On the contrary, the REE concentrations for the Vallorescine “D” facies are systematically higher than those of the Morcles microgranite, which excludes a common origin between both rock types.

Interestingly, the Vallorescine porphyritic granite is also crosscut by microgranitic dykes (Collet et al. 1951; Brändlein 1991; Brändlein et al. 1994) similar in many respects to those of the Morcles area (see e.g. the outcrops exposed north of Les Marécottes, Swiss grid coordinates 2°56'460/1°108'540). Unfortunately, no data are currently available in the literature to directly assess the degree of geochemical similarity between the two types of microgranitic dykes. Further work is planned to fill this gap and bring additional arguments on the possible genetic relationship between the Morcles and Vallorescine microgranites.

To sum up, a common origin between the Morcles and the Vallorescine intrusive bodies is indicated by both geochronological and geochemical data. This observation is further supported by the geographical location of the Morcles microgranitic dykes in the continuation of the Vallorescine intrusion on the northern side of the Rhone Valley, and by the occurrence of potentially equivalent dykes crosscutting the Vallorescine porphyritic granite. The emplacement of the Morcles microgranite was very shallow, as testified by the fine-grained subvolcanic textures of the groundmass. This feature is structurally coherent with the regime of extension that led to the contemporaneous formation of the nearby Salvan-Doré basin over the AR polymetamorphic basement in the late-Variscan period. Based on those observations we suggest that the Morcles microgranite represents the shallow-level counterpart of the Vallorescine porphyritic “H” granite. This assumption is not undermined by the current position of the Vallorescine “H” granite, which outcrops at higher altitudes than the Morcles microgranite. This setting can be explained by the plunging of the AR massif towards the N-E beneath the Helvetic nappes either due to the formation of the Rawil depression structure (von Tscharnier et al. 2016), and/or higher exhumation rates towards S-W (Boutoux et al. 2016).

## 7 Conclusions

On the basis of U–Pb zircon analyses, the intrusion of the Morcles microgranite/rhyolite into the Aiguilles Rouges polymetamorphic basement has been dated at ~303 and ~309–312 Ma. Zircon grains also reveal inherited ages with a major contribution from the Ordovician (Caledonian cycle), and a minor one from the Ediacaran (Pan-African cycle). With an age of 2.3 Ga the oldest zircon is interpreted of Gondwanan origin.

The Morcles microgranite/rhyolite are part of the late-Variscan intrusive bodies, well documented in the Aiguilles Rouges polymetamorphic basement and in the different External Crystalline Massifs of the Alps. Intrusions occurred as dykes in a context of extension that followed the Variscan collision. Extensive anatexis of the crust was triggered by underplating of high-temperature mantle-derived magmas, and, possibly, by intense shearing on large-scale faults.

Geochronological, geochemical and structural arguments point to a common origin for the Morcles and the Vallorescine intrusions, the former being interpreted as the shallow-level counterpart of the latter. As a consequence, both intrusive bodies could be viewed as a single entity extending on either side of the Rhone Valley.

**Acknowledgements** The authors would like to dedicate this article to S. Ayrton (†) who drew our attention to the Morcles microgranite already back in 1990. The XRF results were obtained thanks to the collaborators of the Centre d'Analyse Minérale (CAM) of the University of Lausanne (Switzerland), in particular J.-C. Lavanchy and H.-R. Pfeifer whose help is gratefully acknowledged. We also thank F. Bussy for the many helpful discussions and advices, as well as G. Borel and O. Müntener for administrative support and laboratory access. Finally, we are very grateful to J. F. von Raumer, and an anonymous reviewer for their constructive remarks and suggestions.

## References

- Barbarin, B. (1996). Genesis of the two main types of peraluminous granitoids. *Geology*, 24, 295–298.
- Bertrand, J.-M., Pidgeon, R. T., Leterrier, J., Guillot, F., Gasquet, D., & Gattiglio, M. (2000). SHRIMP and IDTIMS U-Pb zircon ages of the pre-Alpine basement in the Internal Western Alps (Savoy and Piemont). *Schweizerische Mineralogische und Petrographische Mitteilungen*, 80, 225–248.
- Boutoux, A., Bellahsen, N., Nanni, U., Pik, R., Verlaquet, A., Rolland, Y., et al. (2016). Thermal and structural evolution of the external Western Alps: insights from (U-Th-Sm)/He thermochronology and RSCM thermometry in the Aiguilles Rouges/Mont Blanc massifs. *Tectonophysics*, 683, 109–123.
- Boynton, W.V. (1984). Cosmochemistry of the rare earth elements: meteorite studies. In: Henderson, P. (Ed.), *Developments in geochemistry* (pp. 63–114). Amsterdam: Elsevier.
- Bradley, D. C. (2011). Secular trends in the geologic record and the supercontinent cycle. *Earth-Science Reviews*, 108, 16–33.
- Brändlein, P. (1991). Petrographische und geochemische Charakteristika des Vallorescine-Granits, Aiguilles-Rouges-Massiv (Westalpen, Schweiz). Ph.D. Thesis, Erlangen-Nuernberg University, Erlangen, Germany, p. 99.
- Brändlein, P., Nollau, G., Sharp, Z., & von Raumer, J. F. (1994). Petrography and geochemistry of the Vallorescine granite (Aiguilles Rouges massif, Western Alps). *Schweizerische Mineralogische und Petrographische Mitteilungen*, 74, 227–243.
- Bussien, D., Bussy, F., Magna, T., & Masson, H. (2011). Timing of Palaeozoic magmatism in the Maggia and Sambuco nappes and paleogeographic implications (Central Lepontine Alps). *Swiss Journal of Geosciences*, 104, 1–29.

- Bussy, F., Hernandez, J., & von Raumer, J. F. (2000). Bimodal magmatism as a consequence of the post-collisional readjustment of the thickened Variscan continental lithosphere (Aiguilles Rouges-Mont Blanc Massifs, Western Alps). *Transactions of the Royal Society of Edinburgh: Earth Sciences*, 91, 221–233.
- Bussy, F., Péronnet, V., Ulianov, A., Epard, J.-L., & Von Raumer, J. F. (2011). Ordovician magmatism in the external French Alps: witness of a peri-gondwanan active continental margin. In J. C. Gutierrez-Marco, I. Rabano, & D. Garcia-Bellido (Eds.), *Ordovician of the world* (pp. 75–82). Madrid: Instituto Geológico y Minero de España.
- Bussy, F., & von Raumer, J. F. (1993). U-Pb dating of Palaeozoic events in the Mont Blanc crystalline massif, Western Alps. In European Geosciences (Ed.), *Union* (pp. 382–383). Strasbourg: Terra Abstracts.
- Bussy, F., & von Raumer, J.F. (1994). U-Pb geochronology of Palaeozoic magmatic events in the Mont-Blanc crystalline massif, Western Alps. In Symposium basement-cover relationships in the Alps (pp. 514–515).
- Capuzzo, N., & Bussy, F. (2000). High-precision dating and origin of synsedimentary volcanism in the Late Carboniferous Salvan-Dorénaz basin (Aiguilles-Rouges Massif, Western Alps). *Schweizerische Mineralogische und Petrographische Mitteilungen*, 80, 147–167.
- Capuzzo, N., & Wetzel, A. (2004). Facies and basin architecture of the Late Carboniferous Salvan-Dorénaz continental basin (Western Alps, Switzerland/France). *Sedimentology*, 51, 675–697.
- Cas, R. A. F., & Wright, J. V. (1987). *Volcanic successions. Modern and Ancient* (p. 528). London: Chapman & Hall.
- Collet, L.W., Lombard, A., Oulianoff, N., Paréjas, E., Reinhard, M. (1951). 24 Barberine. In Atlas géologique de la Suisse (p. avec notice explicative). Office fédéral des eaux et de la géologie.
- Corsini, M., & Rolland, Y. (2009). Late evolution of the southern European Variscan belt: exhumation of the lower crust in a context of oblique convergence. *Comptes Rendus Geoscience*, 341, 214–223.
- Dobmeier, C. (1996). Geodynamische Entwicklung des südwestlichen Aiguilles-Rouges-Massivs (Westalpen, Frankreich). *Mémoires de Géologie (Lausanne)*, 29, 191.
- Dobmeier, C., Pfeifer, H. R., & von Raumer, J. F. (1999). The newly defined “Greenstone Unit” of the Aiguilles Rouges massif (western Alps): remnant of an Early Palaeozoic oceanic island-arc? *Schweizerische Mineralogische und Petrographische Mitteilungen*, 79, 263–276.
- Egli, D., & Mancktelow, N. (2013). The structural history of the Mont Blanc massif with regard to models for its recent exhumation. *Swiss Journal of Geosciences*, 106, 469–489.
- Egli, D., Mancktelow, N., & Spikings, R. (2017). Constraints from  $^{40}\text{Ar}/^{39}\text{Ar}$  geochronology on the timing of Alpine shear zones in the Mont Blanc—Aiguilles Rouges region of the European Alps. *Tectonics*, 36, 1–19.
- Faure, M., Lardeaux, J.-M., & Ledru, P. (2009). A review of the pre-Permian geology of the Variscan French Massif Central. *Comptes Rendus Geoscience*, 341, 202–213.
- Faure, M., Leloix, C., & Roig, J.-Y. (1997). L'évolution polycyclique de la chaîne hercynienne. *Bulletin de la Société Géologique de France*, 168, 695–705.
- Franke, W., Cocks, L. R. M., & Torsvik, T. H. (2017). The Palaeozoic Variscan oceans revisited. *Gondwana Research*, 48, 257–284.
- Gebauer, D. (1993). The pre-Alpine evolution of the continental crust of the Central Alps - an overview. In J. F. von Raumer & F. Neubauer (Eds.), *Pre-Mesozoic geology in the Alps* (pp. 93–117). Berlin: Springer.
- Gretter, N., Ronchi, A., Langone, A., & Perotti, C. R. (2013). The transition between the two major Permian tectono-stratigraphic cycles in the central Southern Alps: results from facies analysis and U/Pb geochronology. *International Journal of Earth Sciences*, 102, 1181–1202.
- Griffin, W. L., Belousova, E. A., Shee, S. R., Pearson, N. J., & O'Reilly, S. Y. (2004). Archean crustal evolution in the northern Yilgarn Craton: U–Pb and Hf-isotope evidence from detrital zircons. *Precambrian Research*, 131, 231–282.
- Guillot, S., & Ménot, R.-P. (2009). Paleozoic evolution of the External Crystalline Massifs of the Western Alps. *Comptes Rendus Geoscience*, 341, 253–265.
- Guillot, F., Schaltegger, U., Bertrand, J.-M., Deloule, É., & Baudin, T. (2002). Zircon U–Pb geochronology of Ordovician magmatism in the polycyclic Ruitor Massif (Internal W Alps). *International Journal of Earth Sciences*, 91, 964–978.
- Jackson, S.E. (2008). LAMTRACE data reduction software for LA-ICP-MS. In Laser ablation ICP-MS in the Earth sciences: Current practices and outstanding issues. (pp. 305–307). Mineralogical Association of Canada.
- Jackson, S. E., Pearson, N. J., Griffin, W. L., & Belousova, E. A. (2004). The application of laser ablation-inductively coupled plasma-mass spectrometry to in situ U–Pb zircon geochronology. *Chemical Geology*, 211, 47–69.
- Laurent, O., Couzinié, S., Zeh, A., Vanderhaeghe, O., Moyon, J.-F., Villaros, A., et al. (2017). Protracted, coeval crust and mantle melting during Variscan late-orogenic evolution: U–Pb dating in the eastern French Massif Central. *International Journal of Earth Sciences*, 106, 421–451.
- Leresche, S. (1992). Pétrographie et géochimie des microgranites des Monts de Collonges et des roches associées. Unpublished Diploma thesis, Université de Lausanne, Switzerland, Lausanne, Switzerland, p. 96.
- Ludwig, K. R. (2012). User's manual for Isoplot 3.75, A geochronological toolkit for Microsoft Excel. *Berkeley Geochronology Center Special Publication*, 5, 1–75.
- Martínez Catalán, J. R., Fernández-Suárez, J., Meireles, C., González Clavijio, E., Belousova, E. A., & Saeed, A. (2008). U–Pb detrital zircon ages in synorogenic deposits of the NW Iberian Massif (Variscan belt): interplay of Devonian–Carboniferous sedimentation and thrust tectonics. *Journal of the Geological Society*, 165, 687–698.
- Matte, P. (2001). The Variscan collage and orogeny (480–290 Ma) and the tectonic definition of the Armorica microplate: a review. *Terra Nova*, 13, 122–128.
- Meisser, N. (2003). La minéralogie de l'uranium dans le massif des Aiguilles Rouges (Alpes occidentales). PhD thesis, Université de Lausanne, Switzerland, 255 p.
- Meisser, N. (2012). La minéralogie de l'uranium dans le massif des Aiguilles Rouges (1 carte + 183 p.). Matériaux pour la Géologie de la Suisse, Série Géotechnique: Office fédéral de la topographie (Swisstopo), Switzerland.
- Mollex, D. (2003). Le magmatisme basique Carbonifère dans le massif des Aiguilles Rouges. Unpublished post-graduate thesis, Université de Lausanne, Switzerland, Switzerland, 123 p.
- Morard, A., & von Raumer, J.F. (2005). Massif du Mont Blanc et des Aiguilles Rouges-Carte géologique du socle cristallin sans couverture quaternaire. Association des Réserves Naturelles des Aiguilles Rouges, <http://www.naiguillesrouges.org/geologie.html>. Accessed 9 Sept 2017.
- Nakamura, N. (1974). Determination of REE, Ba, Fe, Mg, Na and K in carbonaceous and ordinary chondrites. *Geochimica et Cosmochimica Acta*, 38, 757–775.
- Olsen, S. N., Johnson, C. M., Beard, B. L., & Baumgartner, L. P. (2000). New U–Pb zircon data and constraints on the age and mode of migmatization in the Aar massif, Central Alps. *European Journal of Mineralogy*, 12, 1245–1260.
- Pilloud, C. (1991). Structures de déformation alpines dans le synclinal de Permo-Carbonifère de Salvan-Dorénaz (massif

- des Aiguilles Rouges, Valais* (p. 105). Lausanne: Université de Lausanne.
- Pupin, J.-P. (1980). Zircon and granite petrology. *Contributions to Mineralogy and Petrology*, 73, 207–220.
- Rey, P. F., Burg, J.-P., & Casey, M. (1997). The Scandinavian Caledonides and their relationship to the Variscan belt. *Geological Society, London, Special Publications*, 121, 179–200.
- Rino, S., Kon, Y., Sato, W., Maruyama, S., Santosh, M., & Zhao, D. (2008). The Grenvillian and Pan-African orogens: world's largest orogenies through geologic time, and their implications on the origin of superplume. *Gondwana Research*, 14, 51–72.
- Rolland, Y., Corsini, M., & Demoux, A. (2009). Metamorphic and structural evolution of the Maures-Tanneron massif (SE Variscan chain): evidence of doming along a transpressional margin. *Bulletin de la Société Géologique de France*, 180, 217–230.
- Rolland, Y., Rossi, M., Cox, S. F., Corsini, M., Mancktelow, N., Pennacchioni, G., et al. (2008). <sup>40</sup>Ar/<sup>39</sup>Ar dating of synkinematic white mica: insights from fluid-rock reaction in low-grade shear zones (Mont Blanc Massif) and constraints on timing of deformation in the NW external Alps. *Geological Society, London, Special Publications*, 299, 293–315.
- Schaltegger, U. (1993). The evolution of the polymetamorphic basement in the Central Alps unravelled by precise U–Pb zircon dating. *Contributions to Mineralogy and Petrology*, 113, 466–478.
- Schaltegger, U., Abrecht, J., & Corfu, F. (2003). The Ordovician orogeny in the Alpine basement: constraints from geochronology and geochemistry in the Aar Massif (Central Alps). *Schweizerische Mineralogische und Petrographische Mitteilungen*, 83, 183–195.
- Schaltegger, U., & Brack, P. (2007). Crustal-scale magmatic systems during intracontinental strike-slip tectonics: U, Pb and Hf isotopic constraints from Permian magmatic rocks of the Southern Alps. *International Journal of Earth Sciences*, 96, 1131–1151.
- Schaltegger, U., & Gebauer, D. (1999). Pre-Alpine geochronology of the Central, Western and Southern Alps. *Schweizerische Mineralogische und Petrographische Mitteilungen*, 79, 79–87.
- Scheiber, T., Berndt, J., Mezger, K., & Pfiffner, O. A. (2014). Precambrian to Paleozoic zircon record in the Siviez-Mischabel basement (western Swiss Alps). *Swiss Journal of Geosciences*. doi:10.1007/s00015-013-0156-2.
- Schuster, R., Scharbert, S., Abart, R., & Frank, W. (2001). Permo-Triassic extension and related HT/LP metamorphism in the Austroalpine - Southalpine realm. *Mitteilungen der Gesellschaft für Geologische Bergbaustudien in Österreich*, 45, 111–141.
- Sláma, J., Kosler, J., Condon, D. J., Crowley, J. L., Gerdes, A., Hanchar, J. M., et al. (2008). Plešovice zircon—a new natural reference material for U–Pb and Hf isotopic microanalysis. *Chemical Geology*, 249, 1–35.
- Stampfli, G. M., Hochard, C., Vérard, C., Wilhem, C., & von Raumer, J. F. (2013). The formation of Pangea. *Tectonophysics*, 593, 1–19.
- Stampfli, G. M., von Raumer, J., & Wilhem, C. (2011). The distribution of Gondwana-derived terranes in the Early Paleozoic. In J. C. Gutierrez-Marco, I. Rabano, & D. Garcia-Bellido (Eds.), *Ordovician of the world* (pp. 567–574). Madrid: Instituto Geológico y Minero de España.
- Ulianov, A., Muntener, O., Schaltegger, U., & Bussy, F. (2012). The data treatment dependent variability of U–Pb zircon ages obtained using mono-collector, sector field, laser ablation ICPMS. *Journal of Analytical Atomic Spectrometry*, 27, 663–676.
- Veevers, J. J. (2004). Gondwanaland from 650–500 Ma assembly through 320 Ma merger in Pangea to 185–100 Ma breakup: supercontinental tectonics via stratigraphy and radiometric dating. *Earth-Science Reviews*, 68, 1–132.
- von Raumer, J. F. (1969). Stilpnomelan als alpinmetamorphes Produkt im Mont-Blanc-Granit. *Contributions to Mineralogy and Petrology*, 21, 257–271.
- von Raumer, J. F. (1998). The Palaeozoic evolution in the Alps: from Gondwana to Pangea. *Geologisches Rundschau*, 87, 407–435.
- von Raumer, J. F., Abrecht, J., Bussy, F., Lombardo, B., Ménot, R.-P., & Schaltegger, U. (1999). The Palaeozoic metamorphic evolution of the Alpine External Massifs. *Schweizerische Mineralogische und Petrographische Mitteilungen*, 79, 5–22.
- von Raumer, J. F., & Bussy, F. (2004). Mont Blanc and Aiguilles Rouges—Geology of their polymetamorphic basement (External Massifs, Western Alps, France-Switzerland). *Mémoires de Géologie (Lausanne)*, 42, 203.
- von Raumer, J. F., Bussy, F., Schaltegger, U., Schulz, B., & Stampfli, G. M. (2013). Pre-Mesozoic Alpine basements—their place in the European Paleozoic framework. *Geological Society of America Bulletin*, 125, 89–108.
- von Raumer, J. F., Bussy, F., & Stampfli, G. M. (2009). The Variscan evolution in the External massifs of the Alps and place in their Variscan framework. *Comptes Rendus Geoscience*, 341, 239–252.
- Von Raumer, J. F., Stampfli, G. M., Borel, G. D., & Bussy, F. (2002). Organisation of pre-Variscan basement areas at the north-Gondwanan margin. *International Journal of Earth Sciences*, 91, 35–52.
- von Tscharner, M., Schmalholz, S. M., & Epard, J. L. (2016). 3-D numerical models of viscous flow applied to fold nappes and the Rawil depression in the Helvetic nappe system (western Switzerland). *Journal of Structural Geology*, 86, 32–46.